
Article:
Pessu, F orcid.org/0000-0003-3587-4309, Barker, R, Chang, F et al. (2 more authors) (2021) Iron sulphide formation and interaction with corrosion inhibitor in H2S-containing environments. Journal of Petroleum Science and Engineering, 207. 109152. ISSN 0920-4105

https://doi.org/10.1016/j.petrol.2021.109152

Iron sulphide formation and interaction with corrosion inhibitor in H_2S-containing environments

Frederick Pessu[1], Richard Barker[1], Fakuen Chang[2], Tao Chen[2] and Anne Neville[1]

[1] Institute of Functional Surfaces (iFS), School of Mechanical Engineering, University of Leeds. Leeds. United Kingdom. LS2 9JT.

[2] Exploration and Petroleum Engineering Advanced Research Centre (EXPEC ARC) Saudi Aramco

Corresponding author: Dr Frederick Pessu
School of Mechanical Engineering, University of Leeds, Woodhouse lane, Leeds, United Kingdom. LS2 9JT.
Email address: f.o.pessu@leeds.ac.uk.

ABSTRACT

Corrosion of carbon steel in H_2S-containing environments poses serious challenges to operations in oilfield and geothermal applications. Carbon steels exposed to H_2S-containing environments are often susceptible to pitting and uniform corrosion, and linked to the properties of iron sulphide (FeS) layers that forms at the corroding interface. This paper investigates the corrosion characteristics of carbon steel in H_2S-containing environments focussing on the early stage kinetics of FeS formation and its interaction with corrosion inhibitors (CI). Experiments were conducted in 3.5 and 5.8 wt% NaCl solution at 80°C in 10% H_2S-90% CO_2-containing environments. *In-situ* electrochemical responses were measured using the linear polarisation resistance (LPR) technique. This was combined with post-experiment surface analysis; scanning electron microscopy (SEM) and X-ray diffraction (XRD) to investigate the nature and morphology of formed FeS . 3D surface profilometry was used to investigate the pitting corrosion characteristics of carbon steel caused by FeS interaction with CI. The results show a fast kinetics of FeS formation by direct reduction of $H_2S_{(aq)}$ with a distinct and easily identifiable morphology, and evidence of minimum level of ferrite dissolution. The early stages of FeS formation and its interaction with CI have a strong influence on the overall corrosion characteristics of carbon steel. A dose of 30 ppm of a commercial corrosion inhibitor (CI); salts of nitrogenous molecules with a fatty acid group, at the corrosion interface induced a competition for surface absorption between CI and emerging FeS. Over the 48 h duration of this test, the FeS formation process was delayed and the mechanisms of its formation quickly became the main driver of pitting corrosion. The amount of CI dosed in this study was not able to prevent FeS-induced pitting corrosion attack on the surface.

Keywords: Iron sulphide, carbon steel, pitting corrosion, uniform corrosion and corrosion inhibitor

1. Introduction

The complex electrochemical processes that precedes and directs iron sulphide (FeS) corrosion product formation and evolution [1-3], significantly influence H_2S-induced corrosion of carbon steel. Uniform and pitting corrosion of carbon steel materials used in H_2S-containing environments is related to a combination of complex electrochemical processes occurring at the corrosion interface[3, 4]. H_2S-induced corrosion and FeS formation is believed to be driven by two reaction mechanisms; direct reduction of dissolved H_2S ($H_2S_{(aq)}$) and/or bisulphide ions ($HS^-_{(aq)}$) at the material interface and aqueous corrosion reactions between ferrous species (Fe^{2+}) from the corroding surface and dissolved ionic species[1, 5-7]. The direct reduction reaction mechanism often leads to the formation of mackinawite as a thin chemisorbed corrosion product layer on the surface, while the latter drives the precipitation of crystalline FeS on the surface after saturation levels have been attained[3, 8]. The true kinetics of FeS formation by direct reduction has not been fully investigated. The nature of chemisorbed FeS is still subject to debate.

Several researchers [6, 8, 9] have consistently shown that uniform corrosion rate can become lower as quickly as mackinawite is initially formed. This was observed in short duration (typically 2-3 hrs) experiments at low concentrations of H_2S gas (100-500 ppm) at 30°C [8], and in ~908 ppm of H_2S gas saturated solution at 22°C [9]. In these studies, the aqueous corrosion reactions pathways are not fully accounted for in the corrosion rate measurements and hence limits the value in their conclusions. In the model developed by Zheng et al.[8], for predicting uniform corrosion rate of carbon steel in H_2S-CO_2 corrosion environments, the earliest kinetics of FeS formation was assumed to be non-existent within 2 hrs of the experiment. While this may be true from a thermodynamics standpoint, the true kinetics of FeS formation still remain unclear; particularly in the early

stages, thus making it difficult to model. Dissolution reactions can either occur between the initially formed FeS and other intermediate specie at the corroding interface, and the dissolved H_2S species [10, 11] and/or ferrite ions from corroding surface and dissolved H_2S species. The latter often leads to deposition of different morphology of FeS; usually fluffy in nature, as an outer layer [3]. The transition between both reaction mechanisms is could cause the instability of mackinawite layers, leading to its breakdown and loss of protective properties[4, 11]. Mackinawite is also known to easily transition to other forms of FeS such as pyrrhotite, pyrite, gregite, etc., depending on other process parameters such as pH, temperature, H_2S partial pressure and time, especially for a closed system[4]. Therefore, the protective and/or semi-protective properties of FeS (commonly mackinawite) could be influenced by such transitions to other forms of FeS. The apparent complexities associated with the mechanisms and progression of H_2S-induced corrosion processes is therefore important for the evolution of uniform and pitting corrosion, especially as mackinawite and other forms of FeS could easily act as cathodes[10].

The efficiencies of several mixed-type and anodic-type corrosion inhibitors against corrosion of carbon steel in mixed H_2S-CO_2 environment were recently investigated by Zhang et al[12]. The results showed improvement in inhibitor efficiencies as a result of the fast adsorption process of cationic compounds promoted by dissolved HS^-. This observation, the fast kinetics of FeS formation and the potential for FeS to metamorphose into other forms of FeS could also influence how a commercially available corrosion inhibitor (CI) will interact across the corrosion interface to mitigate both uniform and pitting corrosion components of material degradation. This aspect of FeS – CI interaction during H_2S corrosion is still not clearly understood and needs to be investigated.

This research investigates the kinetics of FeS formation and interaction with a single dose of corrosion inhibitor (CI) (salts of nitrogenous molecules with a fatty acid group) in H_2S-containing environments. The uniform and pitting corrosion behaviour of carbon steel were also investigated in this study. *In situ* electrochemical responses are correlated with FeS formation and interaction with CI. The experiment methodologies also include the correlation of FeS formation and FeS-CI interaction at corrosion interface with corrosion damage mechanisms; uniform and pitting corrosion mechanism. These results will help to improve on current understanding of the process and consequences of FeS formation and interaction with CI at a corroding interface.

2. Materials and Experimental Procedure

The work presented in this paper is based on two separate experiments, both conducted at 80°C:

1. Investigation of the initial stages of H_2S corrosion/FeS formation kinetics over 4.5 h. This was conducted initially in 100% CO_2 gas for 2 hrs and then 10% H_2S – Bal. CO_2 (written as 10% H_2S-CO_2 for the rest of the paper) for another 2.5hrs at 80°C. This experiment was conducted in a 3.5 wt% NaCl and referenced to experiments in 100 % CO_2 and 10% H_2S-CO_2 separately. The focus of this experiment is to access how quickly FeS forms and influences the uniform corrosion behaviour of carbon steel in H_2S-containing environments.

2. Investigation of FeS – CI interaction for 48 h at 80°C and its effect on the corrosion damage mechanisms of carbon steel in 10% H_2S-CO_2-containing environment. In this experiment, *in-situ* electrochemical measurement is combined with post experiment analysis of FeS corrosion products formed and characterisation of pitting corrosion damage. This experiment was conducted in a 1M NaCl solution.

Although the brine NaCl concentration in both experiment 1 and 2 are different, it is important to note that experiment 1 and 2 have not been conducted for direct comparison of research outcomes, but to correlate the underpinning mechanisms of FeS formation kinetics and influence on its interaction with CI.

2.1 General information on corrosion inhibitor

The corrosion inhibitor used in this study is based on the products of reaction of an ethoxylated amine and a dicarboxylic ester[13] and is generally described as salts of nitrogenous bases[14]. This class of CI was developed mainly for corrosion environment dominated by CO_2 corrosion mechanisms where a significant amount of ferrous ions is required to be available at the corrosion interface for effective corrosion inhibition[13]. Corrosion inhibitor film of iron carboxylate is expected to form through the reaction of the ferrous ions with the inhibitor[13]. This preferred method of CI activity makes it a suitable candidate for investigating its interaction with FeS formation. A fixed amount (30 ppm) of CI was used in this study. Details of the experimental matrix in this study is provided in

Table 1.

Table 1: Experimental conditions for investigating corrosion of carbon steel in H_2S-containing corrosion environments

S/N	Scope	Temperature (°C)	NaCl Brine (wt%)	Gas system	Duration (hrs)	pH at start of test	pH at end of test
Exp. 1	FeS Formation Kinetics	80	3.5	100% CO_2	7	3.8±0.2	4.7±0.1
				10% H_2S-CO_2	7	4.30±0.1	4.5±0.3
				100% CO_2 (2 hrs), then 10% H_2S-CO_2 (2.5 hrs)	4.5	3.8±0.2	4.20±0.2
Exp. 2	FeS-Cl interaction	80	5.8	10% H_2S-CO_2	48	N/A	N/A

2.2 Materials

X65 carbon steel samples were used as the working electrodes as part of a three-electrode cell in each experiment. The steel is composed of a ferritic/pearlitic microstructure. The nominal composition of X65 steel is provided in Table 2.

Table 2: X65 carbon steel composition (wt%)

C	Si	P	S	Mo	Mn	Ni	Nb	V	Fe
0.15	0.22	0.023	0.002	0.17	1.42	0.09	0.05	0.06	97.81

Each carbon steel test specimen used was sectioned into 10 mm x 10 mm x 5 mm sections. Wires were soldered to the back of each test specimen and then embedded in a non-conducting resin. In each of the test setups, a total of 5 samples (equivalent to a total of 5 cm^2 of exposed surface area) per litre of test solution is maintained in this study. Details of test setup are described in the next section. Prior to mounting the test samples into the test vessels, the samples were wet-ground up to 1200 silicon carbide grit paper, degreased with acetone, rinsed with distilled water and dried with compressed air before being assembled within the test setup.

2.3 Experiment setup

All experiments described in this section were performed in a 1 litre vessel at atmospheric pressure and 80°C, and repeated for a minimum of 3 times. The pH of each test solution was measured at the start of each tests for each condition after saturation with H_2S-CO_2 gas mixture.

2.3.1 Experiment – 1

The test solutions were deaerated and saturated with CO_2 for a minimum of 12 h and heated up to 60°C. 5 samples were assembled in a 3 electrode cell set up each of which has an exposed surface area equal to 1 cm^2. The test vessels are leaked-tested with 100% CO_2 before heating up to 80°C. Electrochemical measurements are implemented for 2 h before a premixed 10% H_2S-CO_2 gas is introduced into the test vessels for 2.5 h. This approach was implemented to monitor the electrochemical responses associated with early stages of H_2S corrosion and FeS formation. In the control experiments, CO_2 was also used to deaerate the solution for up to 12 h for test in 100% CO_2 for 7 h, while N_2 was used to deaerate the solution for up to 12 hrs for test in 10% H_2S-CO_2 for 7 hrs. The fluctuations in corrosion potential to either more anodic or cathodic values was used to monitor the moment at which H_2S gas being introduced into the test vessel comes in contact with the samples already immersed in a CO_2 or N_2 saturated solution for the first time. The pH was measured at the start and end of each experiments under experiment – 1 as shown in

Table 1.

2.3.2 *Experiment – 2*

This experiment was conducted in a 1 litre autoclave shown in

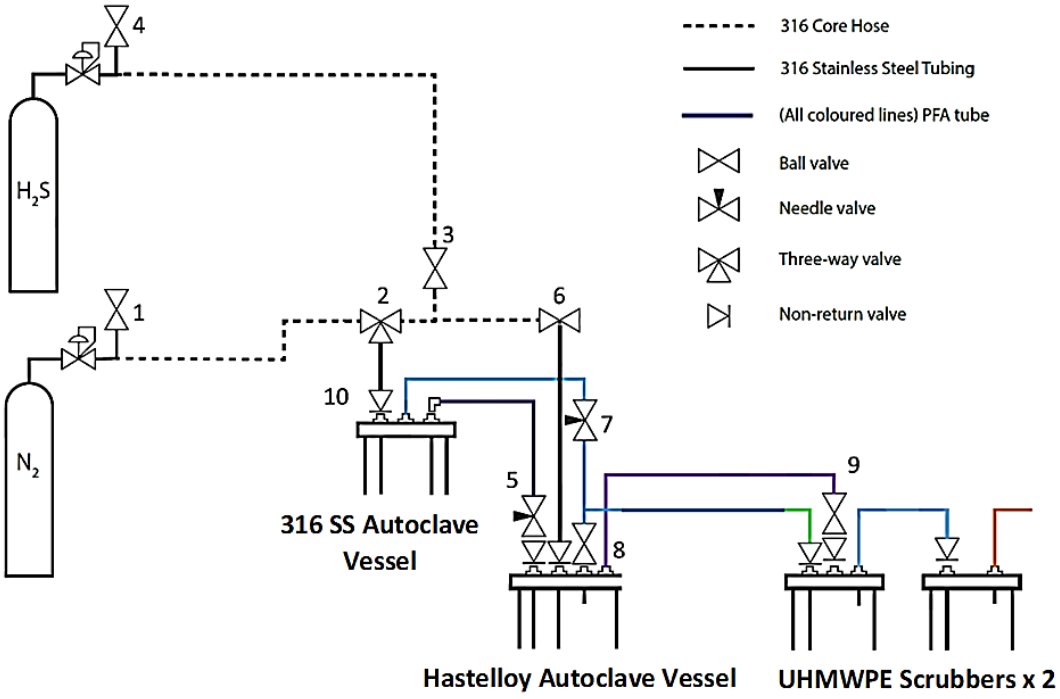

Figure 1. The test solution was deaerated for a minimum of 12 h using N_2 in a 316 SS vessel before it is carefully introduced into an already deaerated 1 litre capacity test vessel containing 5 samples (each with a surface area of 1 cm^2) safely embedded in resin and with wires attached to 3 of the 5 samples for electrochemical measurements. 10 % H_2S-CO_2 gas mixture is introduced into the test solution using valves 4, 3 and 6 (see

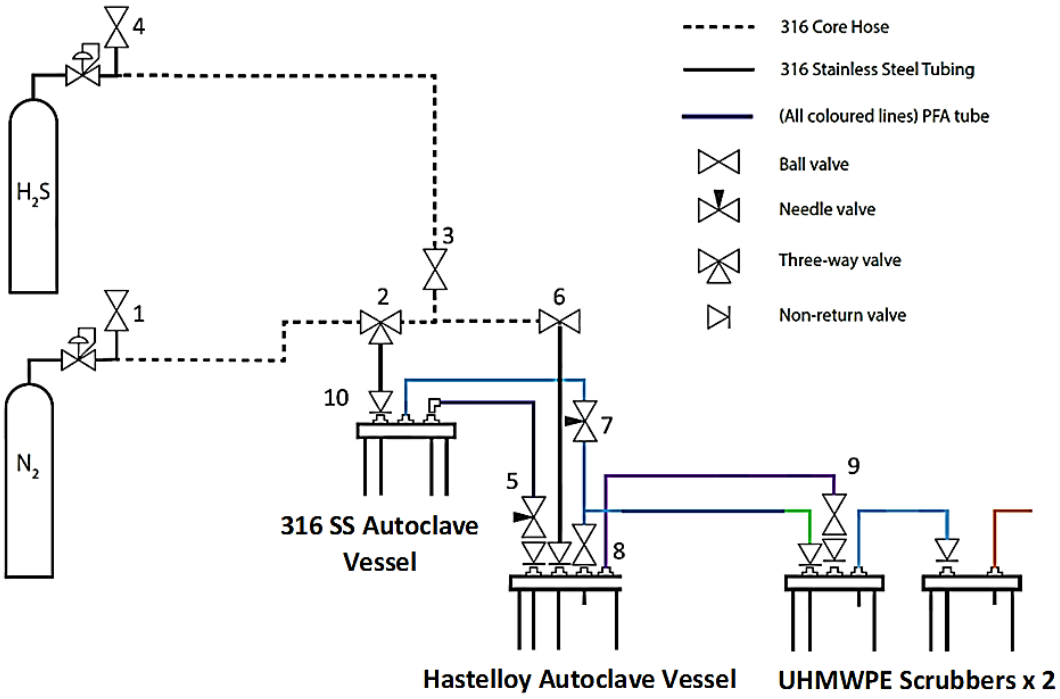

Figure 1) while valves 1 and 2 (in same

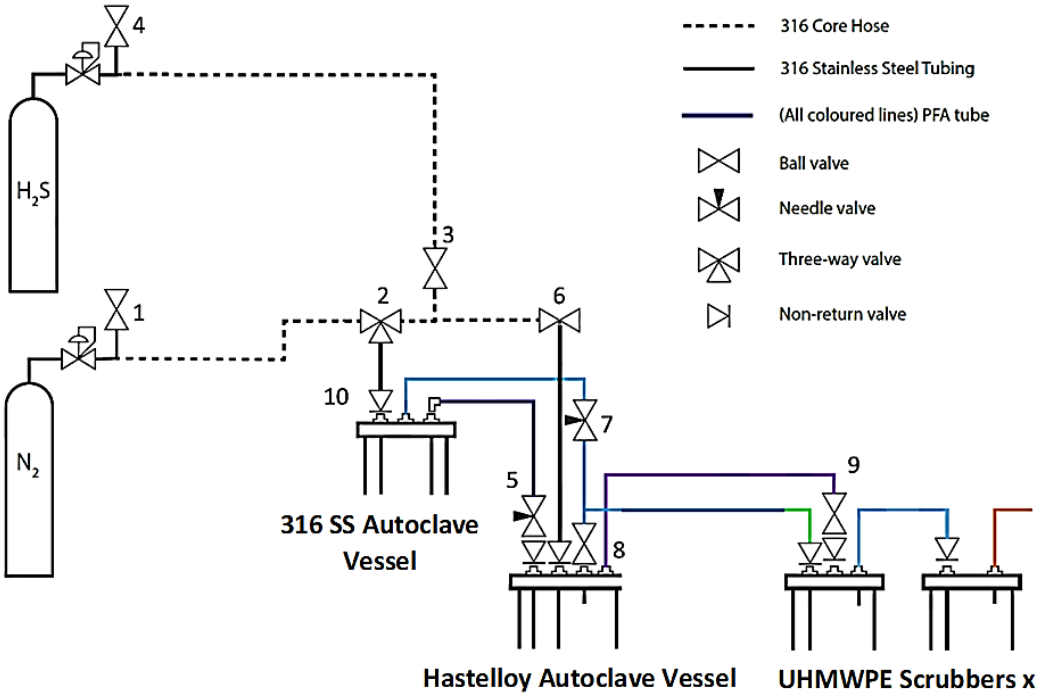

Figure 1) are shut after removal of oxygen. Prior to the transfer of the deaerated solution into the test vessel, the solution was heated to 80˚C in the 316 SS vessel. The exit line of the test vessel was channelled into a 2L 316 SS autoclaves with a PTFE liner containing 10 wt% NaOH and three other polymer vessels containing Jasorb G-15 scrubbing pellets. The corrosion potential is used to monitor the moment at which H_2S gas being introduced into the test vessel comes in contact with the samples already immersed in a N_2 saturated solution for the first time. Corrosion rate measurements start once the H_2S gas supply was turned on.

In experiment – 2, tests with and without CI was performed. Test without CI was used as a reference The CI was introduced into the deaerated solution before being transferred into the test autoclave. This means that the CI is already establishing contact with the material surface before the premixed 10% H_2S-CO_2 gas is introduced. The purpose of this methodology is to investigate the potential competition for the corrosion interface between the CI and FeS and its impact. This is tracked via *in-situ* measurements of electrochemical response over 48 h in combination with post-experiment surface analysis after 48 h. The blank test and test with 30 ppm of CI were repeated three or more times along with *in-situ* electrochemical measurements. Only two repeats were used for post the experiment surface analysis.

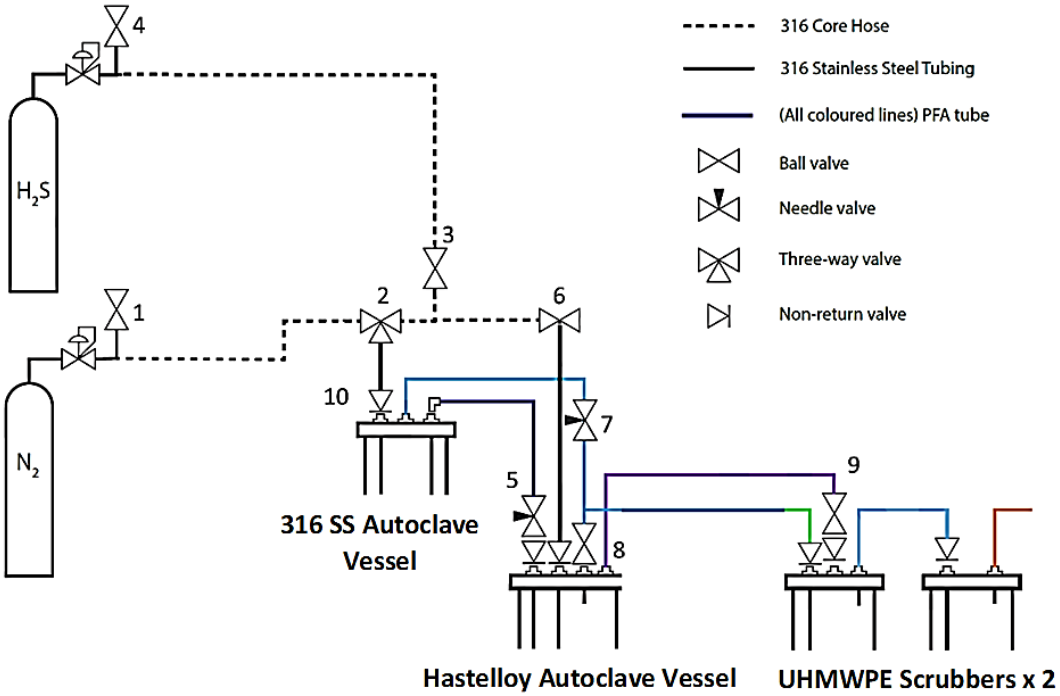

Figure 1: Schematic illustration of H_2S experimental setup used for experiment -2.

2.3.3 Post – experiment sample handling and preparation

In both experiments – 1 and 2, samples were removed for corrosion product characterisation and identification using scanning electron microscopy (SEM) and X-ray diffraction (XRD). Pitting corrosion assessment was carried out only for samples from Experiment – 2. The samples used for pitting corrosion assessment were cleaned with Clarke's solution to remove all traces of corrosion product before using surface profilometry to determine the extent of pitting corrosion on the steel surface. Clarke's solution used consist of 20g of antimony trioxide, 50g of stannous chloride and 1000ml of 37% hydrochloric acid, and prepared in accordance with ASTM[1] Standard G1-03. The sample surface were wiped with a cotton pad soaked in Clarke's solution, washed, air dried, and carefully stored in a de-aerated chamber to avoid oxidation prior to surface analysis. Pitting corrosion analysis was carried out using the NPFLEX 3D[2] interferometer.

2.3.4 In-situ electrochemical measurements

Electrochemical measurements were conducted on one sample per test vessel in all experiments in a three-electrode cell setup. The three-electrode cell comprises of an Ag/AgCl reference electrode and a platinum counter electrode. Electrochemical measurements were made each time the tests were repeated. All electrochemical measurements were conducted using a Gill ACM potentiostat. Linear polarisation resistance (LPR) measurements were performed by polarising each sample every 15 minutes ± 15 mV below and above the open circuit potential (OCP) at a scan rate of 0.25 mV/s to determine the polarisation resistance (R_p). Tafel polarisation measurements were made on test samples from Experiment 1 at the end of each test; after 4.5 and 7 h. Anodic and cathodic sweeps of the Tafel polarisation curves were performed on two different samples in the same test cell, and for conditions in Experiment – 1. Tafel polarisation measurements were used to gain fundamental insights into the kinetics of FeS formation and validate the trend in corrosion rate measurements from the LPR method. Anodic and cathodic sweeps were performed up to ±250 mV about the OCP at a scan rate of 0.25 mV/s. Tafel constants (β_a and β_c) of 120 mV/decade were used in conjunction with R_p and Faraday's Law to determine the *in situ* corrosion rates as a function of time for all experiments in this study.

[1] Trade name

[2] Trade name

2.3.5 *Corrosion product identification*

XRD patterns were collected using a Bruker D8[3] equipped with a LynxEye[4] detector, using a 90 position auto sampler and employing Cu Kα radiation with an active area of 1cm^2 programmable divergence slits. Scans were performed over a range 2Θ = 10 to 70° at a step size of 0.033 per second and a total scan time of ~ 50 minutes. The results were analyzed using X'Pert[5] HighScore software and compared with individual crystal standards from in-house database.

2.3.6 *Characterisation of pitting corrosion damage*

Surface profilometry was deployed in this study to assess pitting corrosion attack for Experiment – 2. Pit depth measurements were conducted in alignment with ASTM G46-94[6][15]. A 3D interferometer was used for obtaining the discrete geometry of pits on over 81% of the steel surface (the remaining 19% represents the edges of the sample). Pits were identified based on carefully chosen thresholds. The thresholds were chosen with reference to the surface roughness of uniformly corroded areas surrounding the pits. This enabled pits with distinct pit diameters, depths, shapes, and areas to be identified and quantified. ASTM G46-94[15] stipulates that an average of the 10 deepest pits and size of deepest pit (relative pit depth measurement after removal of corrosion products) should be used for characterising pitting corrosion damage.

3. Results and Discussion

3.1 H_2S – corrosion; fast iron sulphide formation

Figure 2 to Figure 5 present the results from Experiment – 1 investigating the fast kinetics of FeS formation and its effect on the corrosion interface. The results discussed in this section is referenced to 100% CO_2 and 10% H_2S – CO_2 – containing corrosion environments for the duration of experiments. This experiment was designed to help understand and elucidate the early stage kinetics of H_2S corrosion/FeS formation and the characteristic behaviour of the corrosion interface.

Referring to Figure 2(a) and (b) for corrosion potential and corrosion rate respectively, there is a rapid change in corrosion characteristics with changes in the gas phase composition from 100% CO_2 to 10% H_2S – CO_2 gas mixtures in real time over 4.5 h. The changes in corrosion potential (Figure 2(a)) in 100% CO_2 saturated system over 2 h (before the introduction of 10% H_2S – CO_2 gas mixtures) is similar to the changes within the first 2 h of test in 100% CO_2 system (from 0 – 7 hrs). The corrosion potential starts at ~ -686 and -685 mV respectively and gradually increases in the positive direction to ~ - 680 mV after 2 h for both systems. This stage of a typical corrosion process in 100% CO_2 corrosion systems is usually characterised by the dissolution of ferrite and the establishment of empty cementite layers and results in an increase in corrosion potential[16]. It is well documented that the in 100% CO_2 saturated corrosion environments, ferrite dissolution process at the corroding interface is usually fully established prior to the formation of $FeCO_3$ corrosion products[16, 17]. This usually results in the establishment of corroding surfaces with clearly defined anodic and cathodic microsites that influence the formation of $FeCO_3$ corrosion products[18, 19]. Figure 2(a) and (b) shows that the introduction of 10% H_2S – CO_2 gas mixtures after 2 h in 100% CO_2 corrosion systems completely transformed the mechanism of interaction between an already electrochemically charged corrosion interface and dissolved sulphide species. It can be observed that as soon as the 10% H_2S – CO_2 gas mixtures is introduced into the corrosion environment, the corrosion rate starts dropping within 0.5 h and decreases from ~4.5 mm/yr to ~2.5 mm/yr within the last 2 h of the experiment. This also correlates with the time at which the corrosion potential starts dropping towards more negative potentials (from ~-677 mV to ~-700 mV) over the same time interval. The observed changes in corrosion potential and reduction in corrosion rate confirm an increasing electrochemical interaction between carbon steel and sulphide species[20]. The corrosion rate after 4.5 h (~2.5 mm/yr) closely approaches the average corrosion rate of tests in 10% H_2S – CO_2 gas mixtures for 7 hrs, after 4.5 h (~2 mm/yr) as shown in Figure 2(b).The observed rapid reduction in corrosion potential and corrosion rate in test with 10% H_2S – CO_2 gas after 2 hrs in 100% CO_2 is consistent with results showing a reduction of corrosion rate within 5 minutes in H_2S environment by Ma *et al.* [9] and potentiodynamic polarisation results published by Choi *et al.* [21].

[3] Trade name

[4] Trade name

[5] Trade name

[6] Trade name

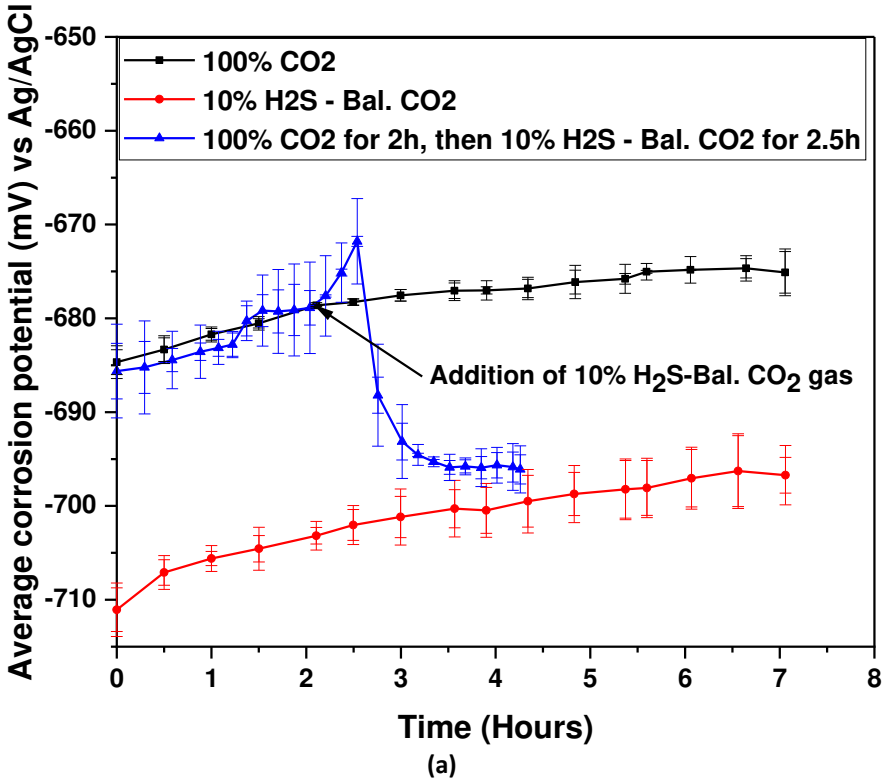

(a)

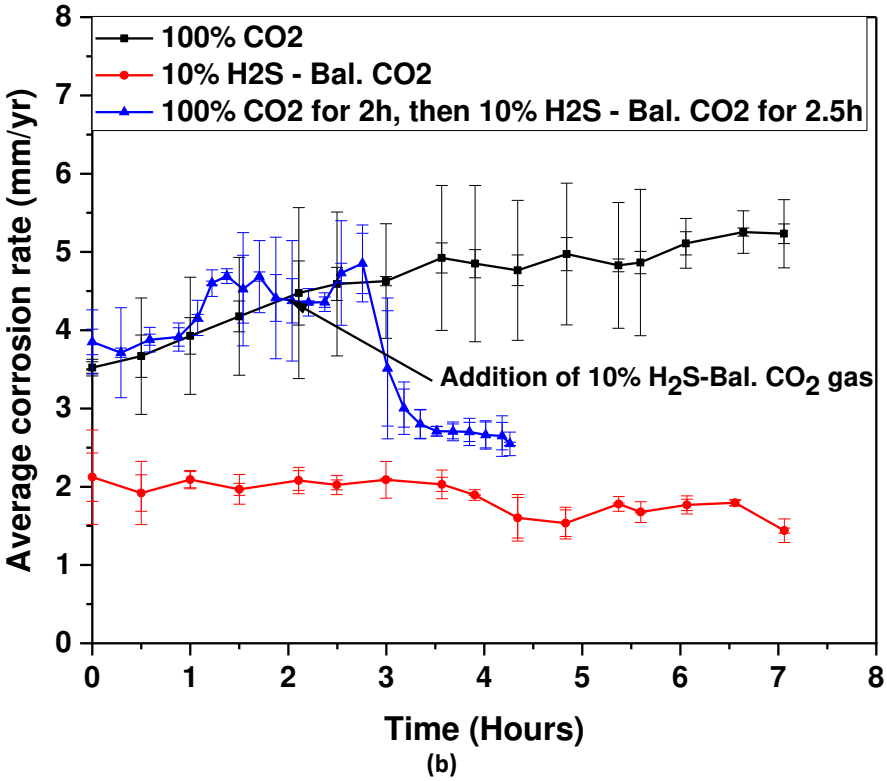

(b)

Figure 2: Plot of (a) corrosion potential and (b) corrosion rate for experiments in 3.5 wt% NaCl solution saturated with 100% CO_2, 10% H_2S – CO_2 over 7 h and test in 100% CO_2 for 2 h and then in 10% H_2S – CO_2 for another 2.5 h at 80°C.

A combination of "direct reduction" of sulphide species at the corrosion interface[1, 22] and the very low solubility limit for FeS formation when compared to that of $FeCO_3$ formation[23, 24] is known to favour the kinetics of FeS formation. The evidence of changes in the redox activities with introduction of 10% H_2S – CO_2 gas mixtures is provided in the potentiodynamic polarisation curves for the three test systems in Figure 3. The cathodic reaction curves are different in shapes to show the influence of 10% H_2S – CO_2 gas mixtures on the cathodic reaction mechanisms at the corrosion interface. The shape of the cathodic reaction line for test initially in 100% CO_2 for

2 h and then 10% H_2S – CO_2 gas mixtures for 2.5 h is distinct from that of test in 10% H_2S – CO_2 gas mixtures for 7 h. This can be described as the "double waves" profile that describes the corrosion mechanisms influenced by both direct reduction of H_2S at the corrosion interface and H^+ reduction at more negative cathodic potential [8]. The "first wave" occurs at more positive cathodic potential (between OCP and ~ -850 mV); representing direct reduction of H_2S, while the "second wave" starts at a more negative cathodic potential (from ~ -850 mV) to represent the H^+ reduction line.

In 100% CO_2 systems after 7 h, the cathodic reaction is controlled by the reduction of H^+ provided by carbonic acid. Similarly, in 10% H_2S – CO_2 gas systems for 7 h, the cathodic reaction is mainly by the H^+ reduction particularly at lower pH[25]. This is why the shape of the cathodic reaction curves are similar for both gas systems after 7 h. The only difference is the suppression of the corrosion current in the 10% H_2S – CO_2 gas systems after 7 h. This is can be related to the fact that FeS has already been formed by direct reduction reaction at earlier times than 7 h during the experiment and as such direct reduction reaction process is no longer dominant. The dominance of H^+ reduction at this stage of the corrosion process is evident in SEM images shown in Figure 4(a) and (b) for tests in 100% CO_2 and 10% H_2S – CO_2 gas systems respectively for 7 h. In Figure 4(a), there is evidence of the evolution of the Fe_3C layer left behind because of ferrite dissolution. In Figure 4(b), Fe_3C is now an inner layer; underneath sparse deposits of FeS layer. This observation shows the competition between ferrite dissolution and FeS formation that has been discussed in a previous publication[2] as an indication of the synergy of CO_2 and H_2S driven corrosion mechanisms in mixed H_2S-CO_2 environments. In this case, the direct reduction of H_2S is likely to have let to the initial formation of FeS. Over the 7 h test duration, the corrosion process became increasingly controlled by H^+ reduction as direct reduction reaction mechanism is suppressed[25]. Thus, as shown in Figure 3, the shape of the cathodic reaction curve for test in 10% H_2S – CO_2 gas systems is of similar shape to that of test in 100 % CO_2 gas systems after 7 h to confirm that both cathodic reaction is strongly influenced by H^+ reduction.

Referring to Figure 3 for test initially in 100% CO_2 for 2 h followed by 10% H_2S – CO_2 gas for 2.5 h, it is evident that the level of suppression of corrosion current is closely approaching that of the test environment with 10% H_2S – CO_2 gas after 7 h. Referring to the cathodic reaction line in Figure 3 and the SEM image in Figure 4(c), there is evidence that the earliest kinetics of FeS formation from tests initially in 100% CO_2 for 2 h and then 10% H_2S – CO_2 gas for 2.5 h is controlled by direct reduction of H_2S at the corrosion surface and not the dissolution of ferrous ions. The cathodic reaction shows a prominent "first wave" at more positive cathodic potential (between OCP and ~ -850 mV) for direct reduction of H_2S [8] and a less prominent "second wave" at more negative cathodic potential (from ~ -850mV) for H^+ reduction. The SEM image in Figure 4(c) shows the presence of FeS rich areas adjacent to areas with little or no FeS but also with minimum revelation of empty Fe_3C. The distribution of FeS across the carbon steel surface can be observed to follow a similar pattern to the distribution of microstructural phases within the steel surface (Figure 4(c)) when compared to the distribution of FeS in Figure 4(b) for test in 10 % H_2S – CO_2 gas mixture after 7 h. This is an indication of minimum ferrite dissolution when compared with the level of exposure of Fe_3C in both 100 % CO_2 and 10% H_2S – CO_2 systems after 7 h. Therefore, the shape of the cathodic reaction line in Figure 3 represents redox activity mainly controlled by direct reduction of H_2S at the steel surface and the corresponding FeS formed is not driven by the saturation of the corrosion interface with ferrous ion (Fe^{2+}) and dissolved sulphide species.

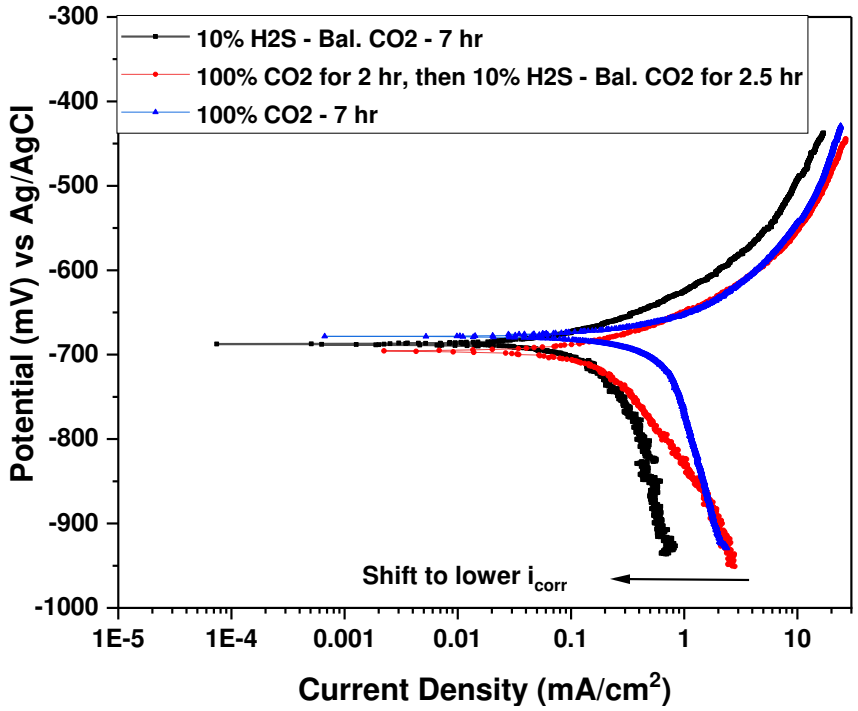

Figure 3: Potentiodynamic curves for experiment in 100% CO_2 for 7 h, 100% CO_2 for 2h and then with 10% H_2S – CO_2 for another 2.5 h, and 10% H_2S – CO_2 for 7 h.

The SEM images in Figure 4(b) and (c) for tests in 10% H_2S – CO_2 gas after 7 h and initially in 100 % CO_2 for 2 h and then 10% H_2S – CO_2 gas for 2.5 h, respectively, also show different physical and morphological features of FeS formed. This correlates well with the dominating cathodic reaction mechanisms in both systems. FeS formed mainly by direct reduction of H_2S at the corroding surface emerges as a chemisorbed (amorphous –like) layer[10] as shown in Figure 4(c) for tests initially in 100 % CO_2 for 2 h and then 10% H_2S – CO_2 gas 2.5 h. With increasing experimental time and competition between direct reduction and an increasingly dominant H^+ reduction reaction, FeS formed is likely to become more crystalline[2, 3]. This is confirmed by the XRD patterns in Figure 5. The XRD pattern shows a weak peak for FeS at 17.92°, 30.33° and 39.20 2° for Bragg diffraction angles of mackinawite in test initially in 100 % CO_2 for 2 h and then 10% H_2S – CO_2 gas for 2.5 h when compared to the XRD pattern for FeS formed in only 10 % H_2S – CO_2 gas mixture from 0 – 7 hrs; showing strong peaks for mackinawite at 17.92°, 30.33° and 39.20 2°. These results therefore provides new and important insights into the mechanism driving the earliest stages of H_2S corrosion and FeS formation beyond what is currently available in the literature.

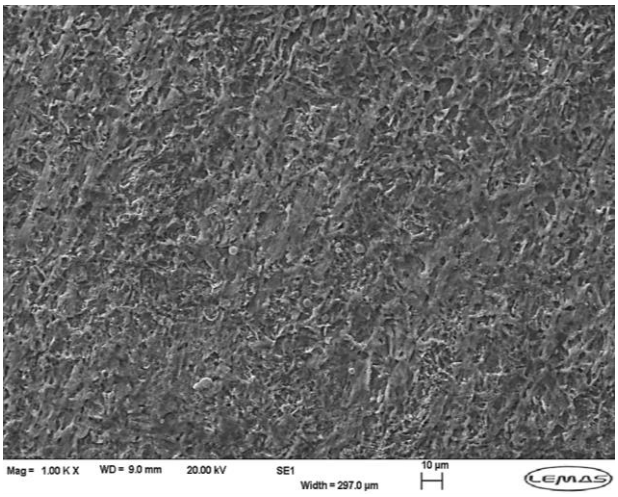

(a)

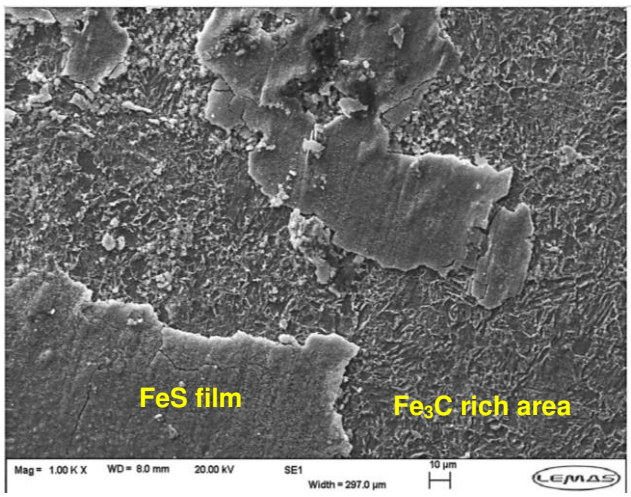

(b)

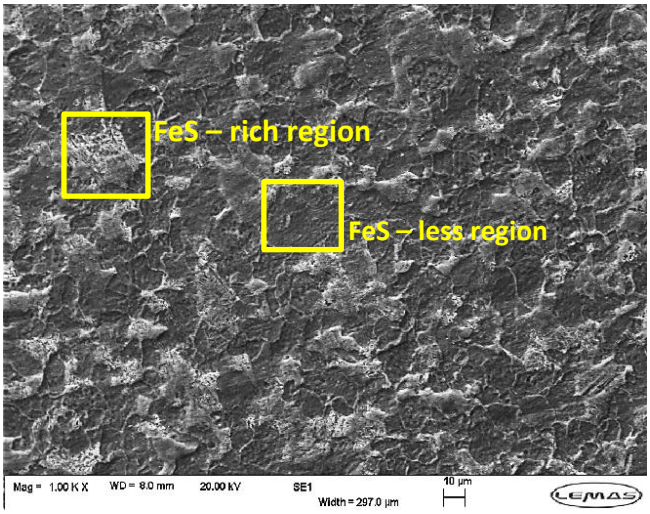

(c)

Figure 4: SEM Images of FeS corrosion products deposited on carbon steel after immersion in 3.5 wt. % NaCl solution saturated with (a) 100% CO_2 after 7 h (b) 100% CO_2 for 2 h and then in 10% H_2S – CO_2 for another 2.5 h and (b) 10% H_2S – CO_2 after 7 h.

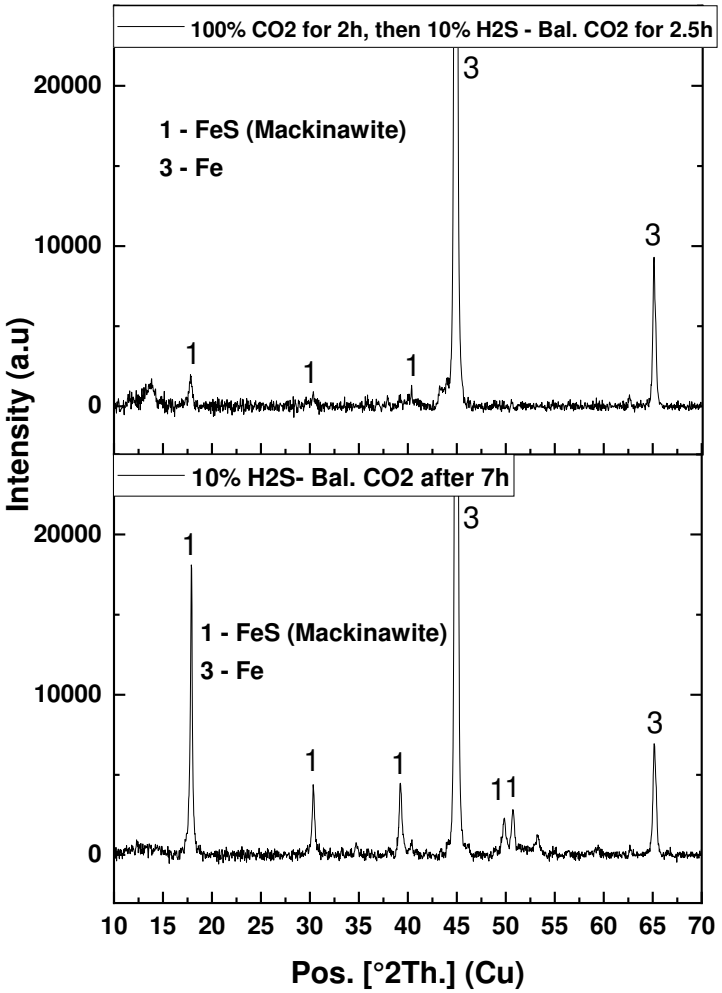

Figure 5: XRD pattern showing the type of FeS deposited on carbon steel after immersion in 3.5 wt% NaCl solution saturated with 100% CO_2 for 2 h and then with 10% H_2S – CO_2 for another 2.5 h, and 10% H_2S – CO_2 for 7 h.

3.2 H_2S – corrosion; iron sulphide formation and Iron sulphide – corrosion inhibitor (CI) interaction

This section investigates the interaction of a fixed concentration (30 ppm) of corrosion inhibitor (CI); made from reaction of an ethoxylated amine and a dicarboxylic ester, with H_2S corrosion and FeS formation process of carbon steel in 10% H_2S – CO_2-containing environment over 48 h. The results discussed in this section are

referenced to a blank test; in 10% H_2S – CO_2-containing environment without CI. The corrosion rate and corrosion potential for tests with and without (CI) is presented in

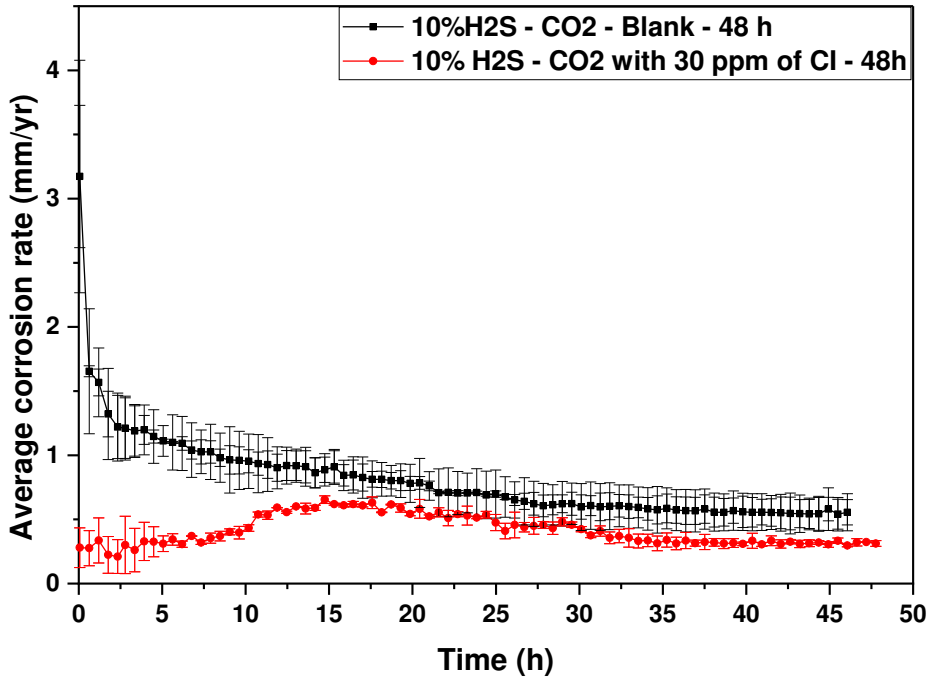

(b)

Figure 6(a) and (b), respectively.

Referring to

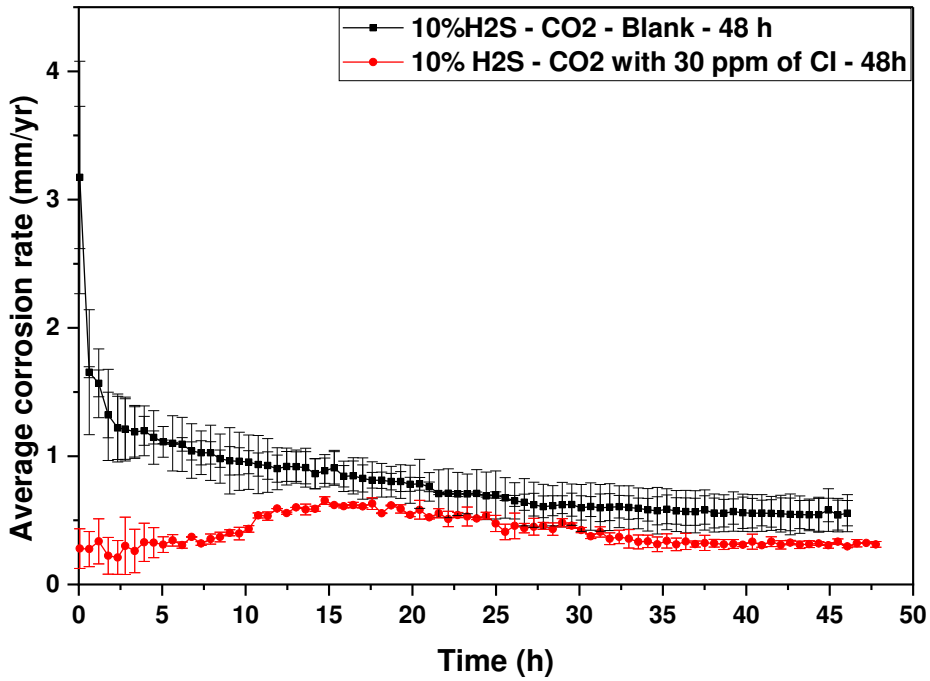

(b)

Figure 6(a), the corrosion potential starts at a more positive value (~ -620mV) for test with CI from the start of tests than the blank test at ~-670 mV due to the establishment of initial CI film on the surface [12, 26]. This process precedes the introduction of 10% H_2S – CO_2 gas mixture into the corrosion environment (see section on details

of experiment – 2). A further increase in corrosion potential from ~-620 mV to ~-600 mV was also observed between 0 – 5 hrs. This correlates with periods of lower corrosion rates (at ~ 0.25 mm/yr) than in the blank tests (at ~1.25 mm/yr) (see

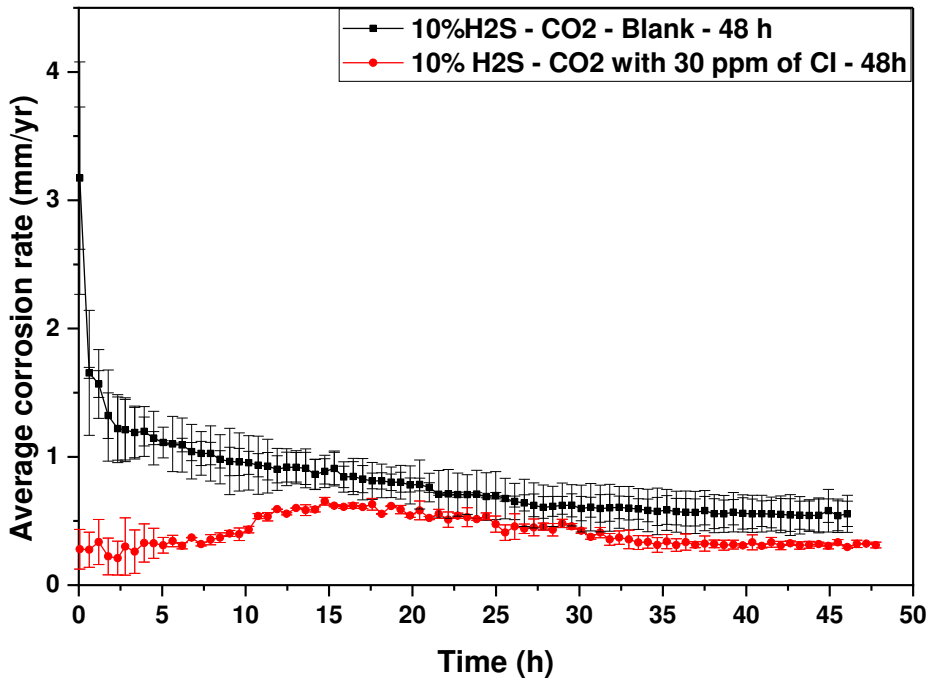

(b)

Figure 6(b)) caused by the introduction of CI in N_2-saturated solution before making contact with the sample surface and prior to introduction of H_2S-containing gas mixtures. This methodology was used in this study because the chosen CI inhibits corrosion through the formation of an iron carboxylate film by reacting with ferrous ions [13]. This will require substantial availability of ferrous ions at the corrosion interface from a preceding ferrite dissolution process. Referring to the results from experiment – 1 in this study, the earliest kinetics of FeS formation will require minimum ferrite dissolution and hence minimum corrosion of the metal surface prior to CI interaction. This scenario therefore presents the ideal case for understanding how CI and the fast kinetics of FeS formation competes for the corrosion interface.

Referring to

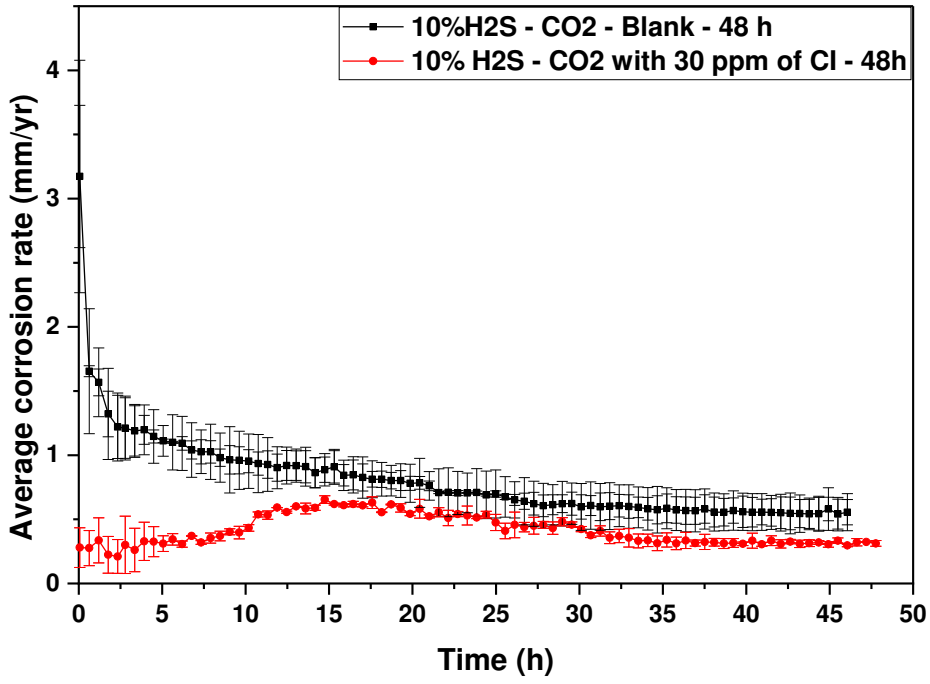

(b)

Figure 6 (a) and (b), the results of increase corrosion potential in the more anodic direction and lower corrosion rate for test with CI than in the blank test from this study is consistent with the results showing the effect of the activity of anodic inhibitors used in combined H_2S-CO_2 corrosion from potentiodynamic measurements at 60°C[12].

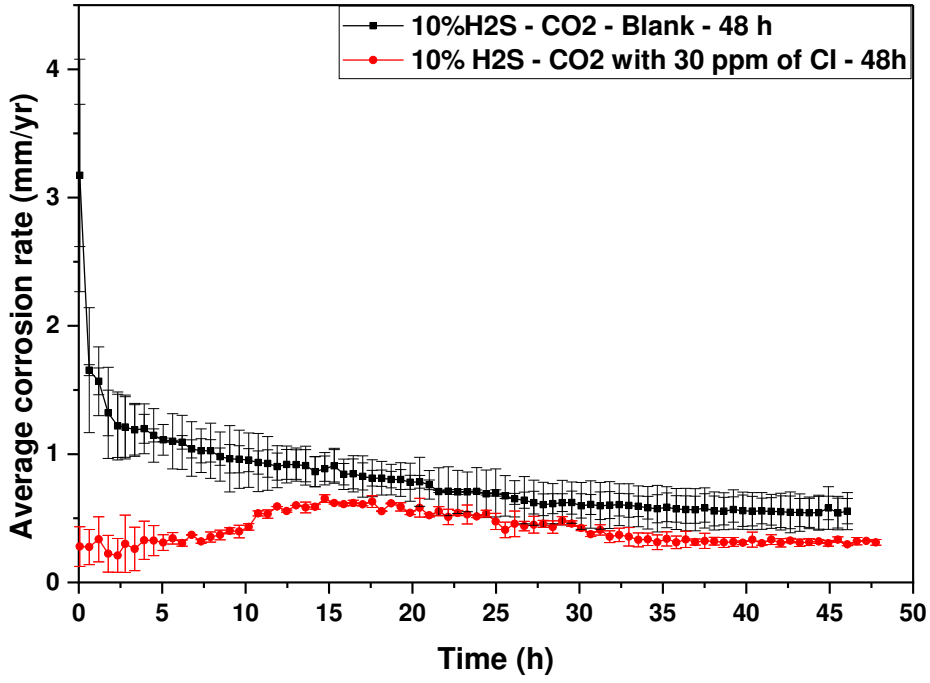

(b)

Figure 6(b) shows a ~58% reduction in corrosion rate (from ~3 mm/yr to ~1.25 mm/yr) between 0 – 5 hrs in the blank test to highlight the inhibitive capacity from established FeS layer on the steel surface. The kinetics and impact on corrosion characteristics of carbon steel in this case is similar to the fast kinetics of FeS formation already established in this paper. This trend of reduction in corrosion rate in the blank test continued slowly until after 30 h when the corrosion rate remained constant at ~0.6 mm/yr until the end of the test. During this process, the corrosion potential of the blank test showed a steady increase towards positive potential as

evidence of the gradual and continuous build-up of FeS layer on the corrosion interface shown by the SEM image in Figure 7(a) and (b) for repeated tests. Although the SEM images appeared to be loosely held and at times "fluffy" from the top view, it is clearly able to suppress the uniform corrosion rate by up to 80% within 48 h by creating some interfacial barrier between the corroding steel and the environment.

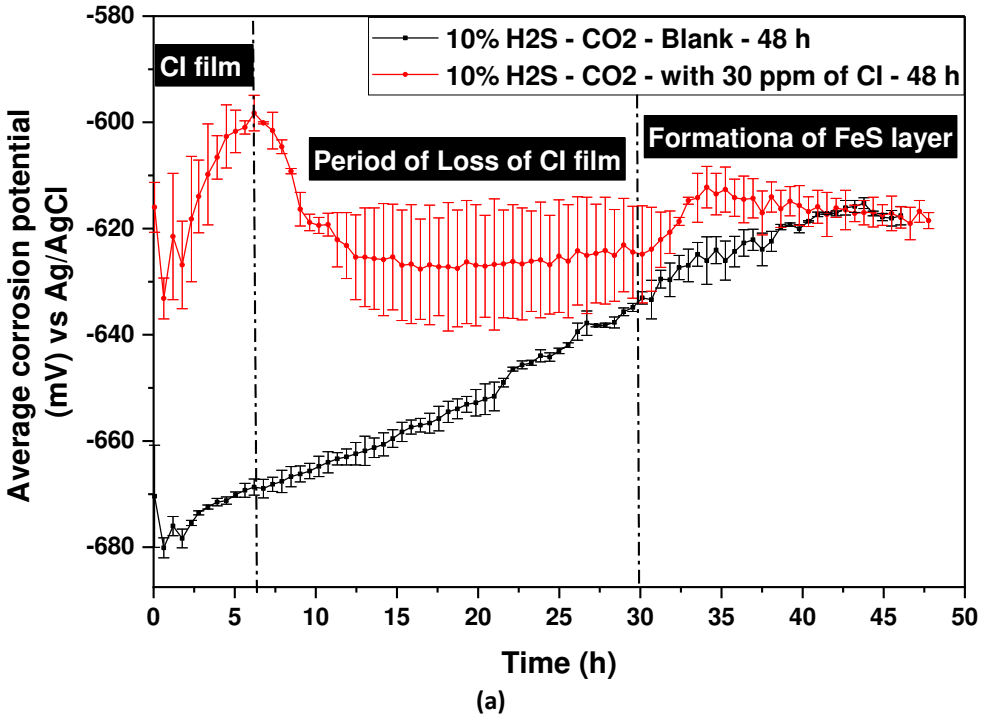

Figure 6: Plot of (a) corrosion potential and (b) corrosion rate for experiments in 10% H_2S – CO_2 over 48 h with 0 ppm (blank) and 30 ppm of Cl.

With respect to tests with 30 ppm of Cl, the corrosion potential starts decreasing between 5 and 15 h towards more negative potential values (see

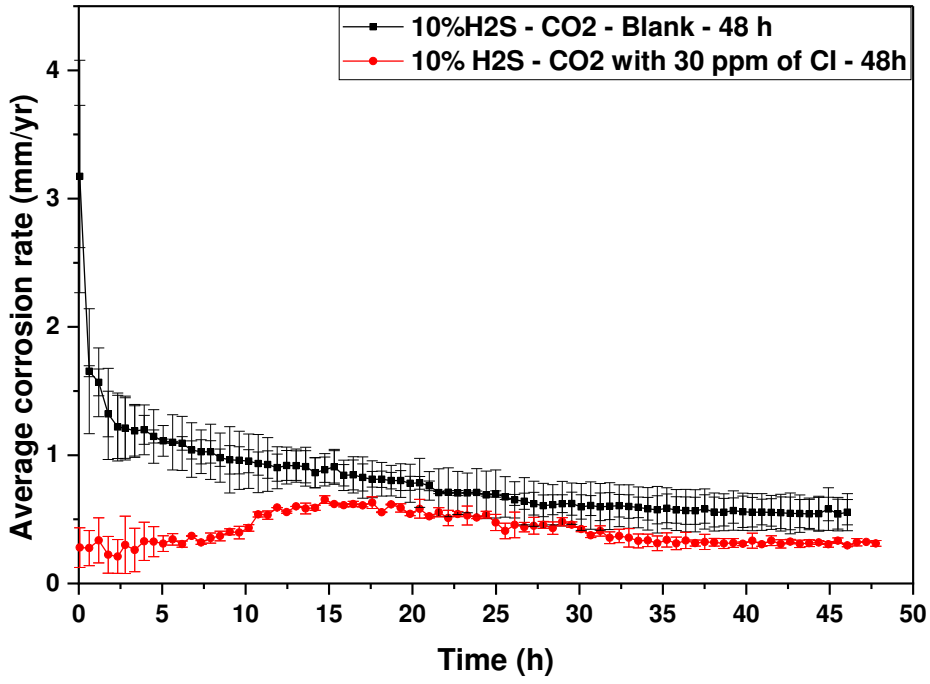

(b)

Figure 6(a)) just as the corrosion rate in

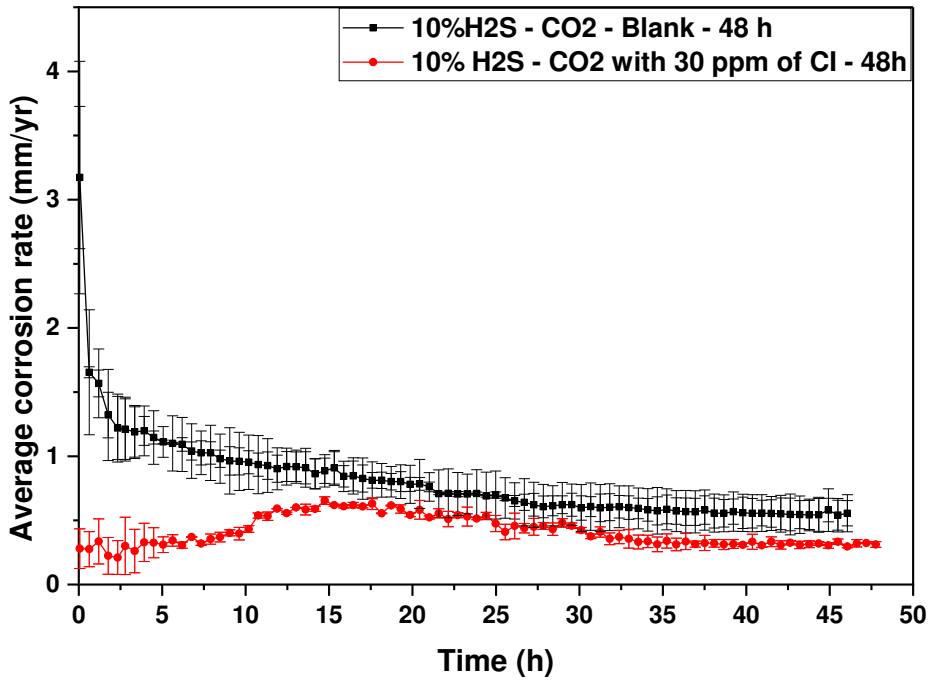

(b)

Figure 6(b) increases threefold to ~0.75 mm/yr. The corrosion potential and corrosion rate remained largely constant from 15 to 30 h before a new slight increase in corrosion potential and a corresponding slightly lower but stable corrosion rate; at ~0.5 mm/yr, is achieved at the end of the test. The reduction in corrosion potential and corresponding increase in corrosion rate between 5 and 15 h is caused by the deterioration of initially formed CI film. This can create opportunities for dissolved sulphide species to interact with the corroding surface for the first time and kick-start the first stage of FeS formation process. Referring to the preferred mechanism of CI interaction, the fast kinetics of FeS formation has prevented the formation of a more resilient iron carboxylate film by suppressing ferrite dissolution and reducing the availability of ferrous ions. It has been

proposed[13] for this particular CI that CI film coverage could also become non-uniform if substantial corrosion of the interface is not allowed prior to its interaction with the CI. In other studies, it was also observed that initially formed CI film can also become weakened by the interaction of active components of CI film with HS^- [12].

The FeS corrosion product observed in test with CI after 48 h is largely amorphous/non-crystalline as shown in the SEM image in Figure 7(c) and (d). This morphology of FeS is usually associated with the earliest stages of FeS formation kinetics. This is confirmed by the similar morphology of FeS formed in 10% H_2S – containing systems previously shown in this paper after 4.5 and 7 h in Figure 4(a) and (b) respectively. It is important to note that it is still unclear from this study the exact time the corroding interface makes its first contact with dissolved sulphide specie in the presence of CI layer. The results from electrochemical responses (

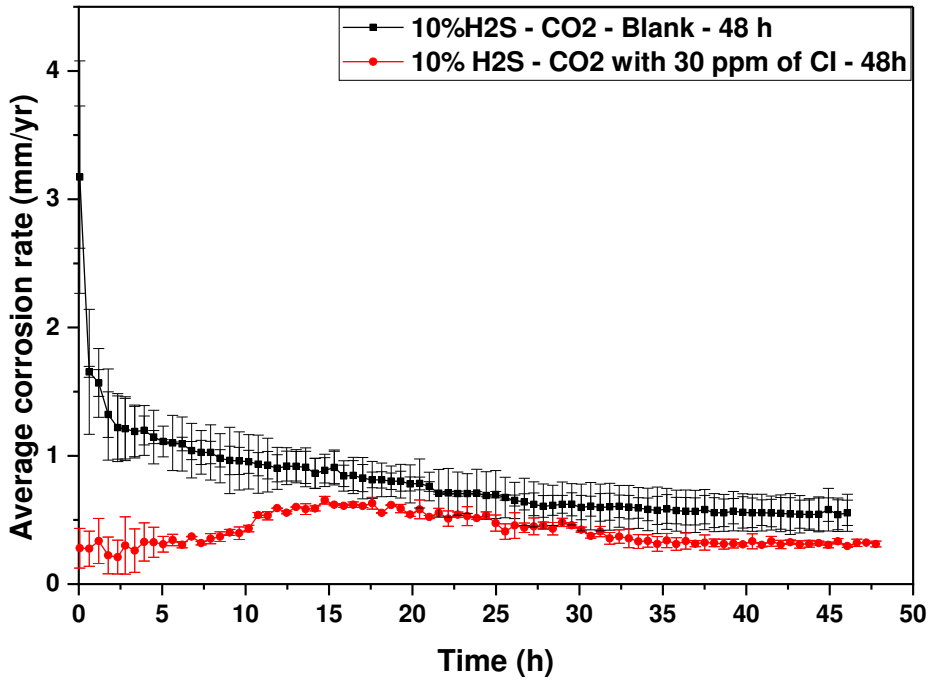

(b)

Figure 6(a) and (b) and SEM images (Figure 7(c) and (d)) strongly suggests that the interaction of the corroding interface and dissolved sulphide species is at its earliest stages after a prior establishment of CI film. This has led to the formation of an amorphous FeS film with evidence of polishing marks from the sample still imprinted and retained on the FeS layer. This morphology of FeS is characteristic of FeS formed by direct reduction of H_2S at the steel surface as already shown in this study. In this instance, the use of CI before the introduction of 10% H_2S – CO_2 gas mixture is observed to have inhibited and delayed the initial formation of FeS, and restrict the morphology of FeS to an amorphous layer when compared to the expected FeS morphology observed from the blank test in Figure 7(a) and (b). The fast kinetics of FeS formation once the dissolved sulphide species makes contact with steel sample also prevents the availability of ferrous ions at the corrosion interface to ensure the development of a more adherent CI film. Once CI layer is successfully displaced from the corrosion interface (between 5 – 15 h), FeS formation kinetics start dominating the interfacial activities, as depicted by the corrosion rate and corrosion potential profiles in

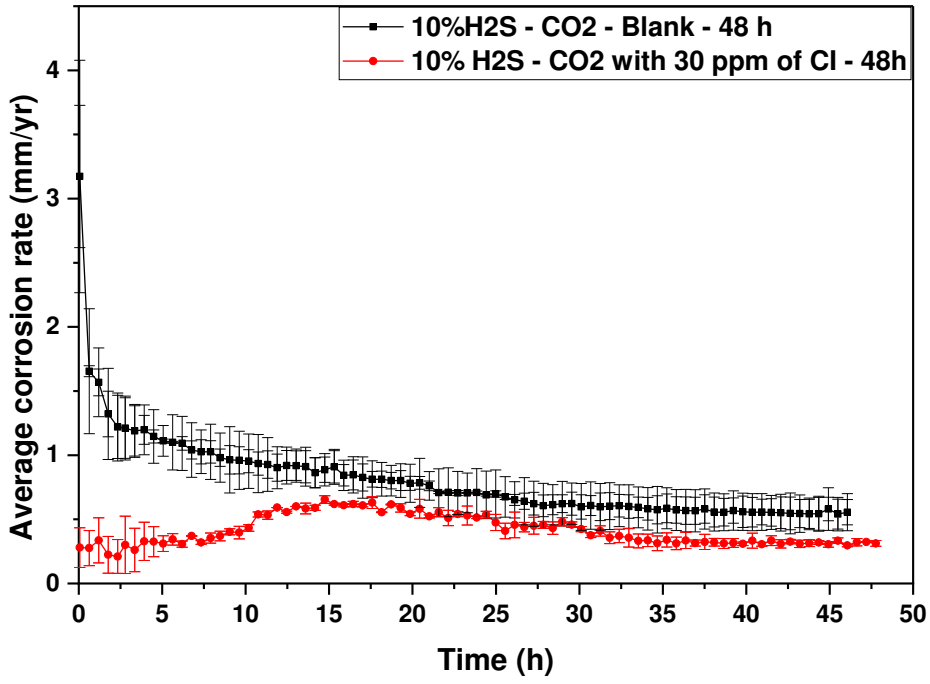

(b)

Figure 6(a) and (b). It is important to note that the *in situ* transition from Cl controlled corrosion interface to FeS controlled corrosion interface in a single experiment has also had the overall impact of suppressing cumulative material loss from uniform corrosion of the carbon steel sample over 48 h. This is supported by the evidence in Figure 2 and Figure 3 that shows how FeS corrosion products can influence the corrosion characteristics of the corroding surface.

The influence of Cl interaction and competition for the corroding steel surface with FeS is also supported by the weak peaks for amorphous FeS formed in test with Cl (mackinawite) on the XRD pattern in Figure 8 in comparison to the strong peaks for largely crystalline FeS (mackinawite) formed in the blank test. The intensity of XRD peaks for FeS formed in test with Cl (Figure 8) is in the same range as the XRD peaks for test initially in 100% CO_2 for 2 h and then 10% H_2S – CO_2 for another 2.5 h (Figure 5). There is also an observed protuberance within the FeS film in Figure 7(c) and (d) for test with Cl. Some of the regions with protuberance showed features that indicate the occurrence of either FeS film rupture and/or collapse (Figure 7(c) and (d)) under some form of internal pressure. These kind of protuberances can be linked to internal epitaxial stresses built-up as a result of the particular mechanism of mackinawite formation at this stage of the corrosion process. Mackinawite scales are known to be of larger volumes than the volume of Fe^{2+} consumed for its formation. It is believed that a larger volume fraction of mackinawite is being formed from a smaller volume fraction of consumed Fe^{2+} to introduce such internal stress effects. The ratio of these volume fractions is usually described as the Pilling-Bedworth (P-B) ratio[27]. These observation highlight the complex interaction between Cl and FeS corrosion product layer that is still not clearly understood and will still require significant research attention and a robust research program to build on the understanding developed in this study.

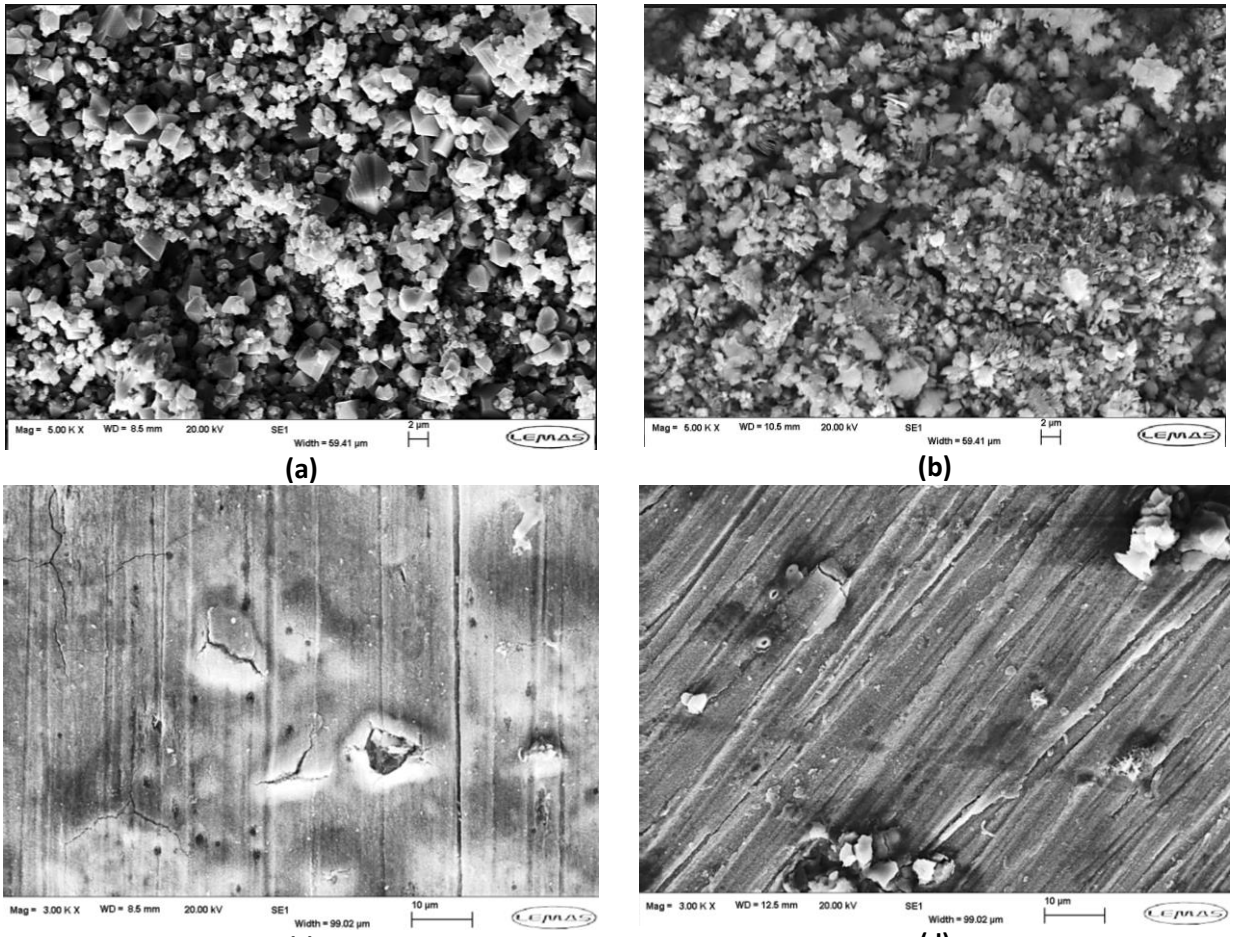

Figure 7: SEM Images of FeS corrosion products deposited on carbon steel in 10% H_2S – CO_2 after 48 h (a) blank (b) blank - repeat (c) with 30 ppm of CI and (d) with 30 ppm of CI – repeat.

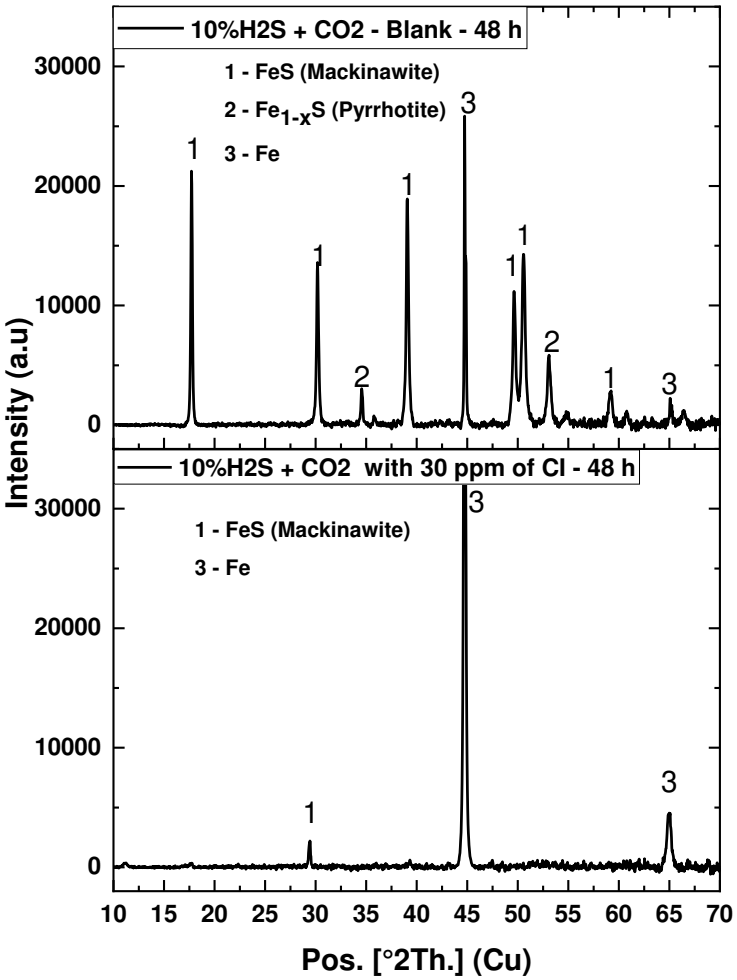

Figure 8: XRD pattern showing the type of FeS deposited on carbon steel in 10% H_2S – CO_2 after 48 h.

3.3 Pitting corrosion; the effect of corrosion inhibitor (CI) – iron sulphide interactions

Figure 9 presents the estimated thickness loss linked to uniform corrosion, depth of deepest pit and average of 10 deepest pits from tests conducted in 10% H_2S – CO_2-containing environment over 48 h, with and without 30 ppm of CI. Data on thickness loss estimated from uniform corrosion is based on the assumption that the localised redox reactions within these pits over 48 h are relatively insignificant when compared to the rate of material loss from the rest of the corrosion interface captured in the electrochemical responses. It is also believed that most ferrous ions linked to the uniform corrosion rate are captured in the build-up of FeS.

Referring to Figure 9, the depth of the deepest pit and the average pit depth is twice as high in test with CI as the blank test while the estimated uniform corrosion contribution is half as much as the blank test. As discussed earlier, the competition for persistency of CI film and H_2S related redox activity for the corrosion interface led to a weakened CI layer and the formation of a semi protective and non-crystalline FeS layer. The SEM images shown in Figure 7(c) and (d) clearly show that the mechanism of formation of the resulting FeS is susceptible to rupture and/or failure, leading to the loss of film integrity when compared to the FeS formed in the blank test (Figure 7(a) and (b)). The loss or partial loss of CI layer is known to be a prolific precursor for pitting initiation[28]. However, when such loss of CI occurs (typically when CI is dosed below the optimum concentration), and precedes the formation of a FeS layer prone to rupturing, it creates the necessary conditions for pit corrosion damage to dominate the material loss mechanism. Visual evidence of pitting corrosion damage (which focuses on the identified deepest pit on an entire exposed surface) is presented for the blank test in Figure 10(a) and for tests with 30 ppm of CI in Figure 10(b) and (c).

Referring to Figure 10(a) to (c), the areas surrounding the pits for test with CI appear to be well protected compared to the blank test. This is due to the combined effect of partial loss of initial CI film and the emerging

FeS layer. The level of protection of surfaces surrounding the pits suggest that the transition from a weak CI film to a semi – protective FeS layer still ensures substantial suppression of uniform corrosion in areas on the steel surface where either the CI film was initially adherent and/or the FeS layer has not been ruptured. It also shows that the rate of deterioration of initial CI film and the formation of FeS layer were not occurring at the same rate across the entire corrosion interface. This is a recipe for the emergence of local galvanic cells, which is enhanced by the electrochemically active nature and electronic properties of FeS corrosion products [10, 29] to support pitting corrosion[30]. Lower depth of pits were observed in the blank test because of the porous nature of the FeS corrosion product. This also implies that the migration of precipitable sulphide species can continue to interact with the base steel to drive ferrous dissolution and recede the reference surface underneath the corrosion product layer. One of the consequences of increased ferrite dissolution is the increased build-up of FeS corrosion products on the surface as shown in Figure 7(a) and (b) and supported by evidence of evenly spread areas on the steel surface with only micro–pits and uniform corrosion. It is likely that subsequent depositions to the FeS layer will continue to supress the ferrous dissolution process and potentially support the growth of these micro–pits with time. These conclusions are supported by the pit count and pitting factor presented in Figure 11(a) and (b), respectively. Pit count data is based on a pit depth threshold of 6 µm and shows a higher number of pits in test with CI than in the blank. The pitting factor is higher for test with CI than the blank test to corroborate the trend in high pit penetration depth and pit count for tests in wit CI than the blank test. This highlights the significant impact of the competitive redox activity between CI and FeS at the corrosion interface on the mechanisms of material loss in H_2S – containing corrosion systems.

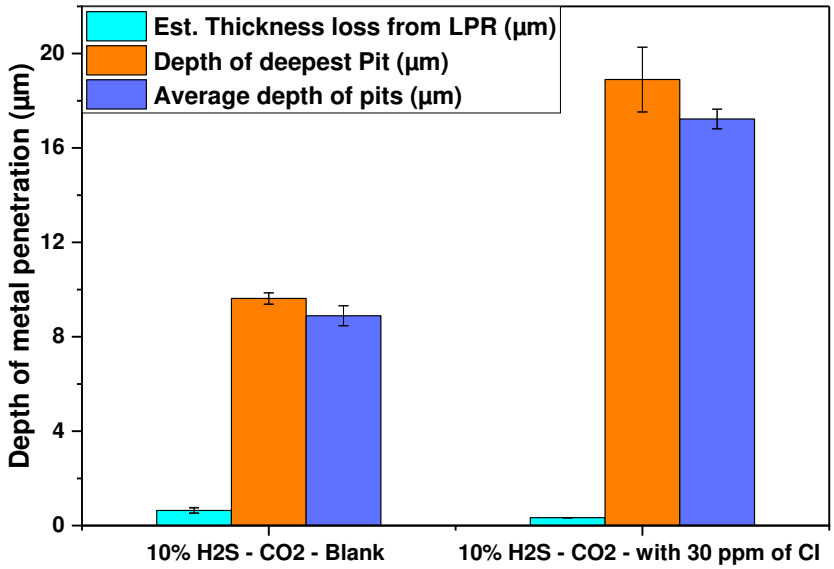

Figure 9: Graph of the thickness loss to general corrosion, the size of deepest pit and the average of the 10 deepest pits on carbon steel in 10% H_2S – CO_2 with 0 and 30 ppm of CI after 48 h. Error bars on pit size data are based on two (2) pit characterisation on samples from two repeatable experiments.

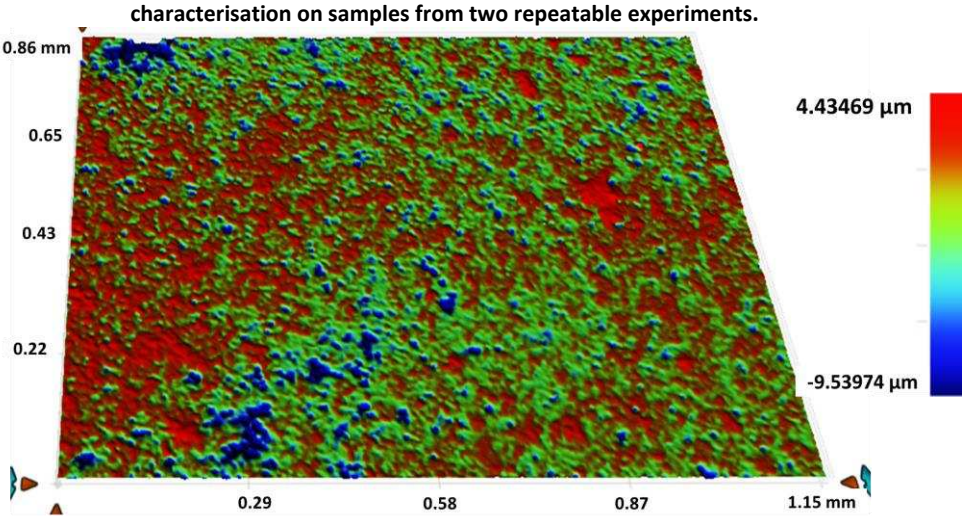

(a)

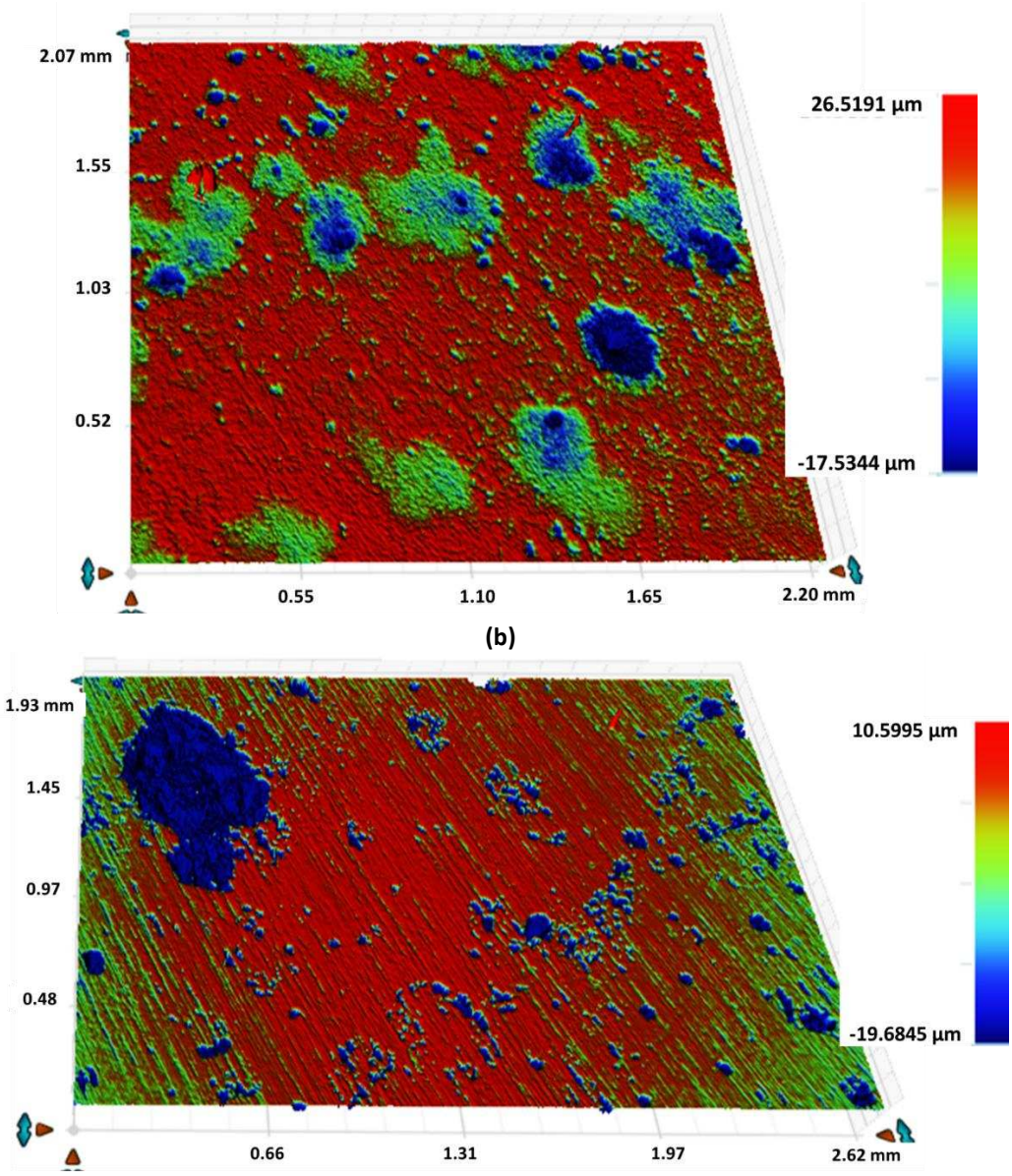

Figure 10: 3D image of the deepest pit on carbon steel in 10% H_2S - CO_2 after 48 h (a) 0 ppm (Blank), (b) with 30 ppm of CI and (c) repeated test with 30 ppm of CI.

The pitting factor (P_f): is used to reflect the relative contribution of corrosion damage mechanisms; pitting and uniform corrosion to metal loss and defined in ASTM standard G46-94[31] as:

Pitting Factor; $$P_f = (\frac{P_d}{P_u})$$ **Equation 1**

Where P_d is the total material penetration (µm) for the exposed surface area (sum of depth of deepest pit (d_{max}), (after removal of corrosion products) plus the estimated thickness loss (µm) from uniform corrosion rate measurement (termed P_u), i.e, $P_d = P_u + d_{max}$. A pitting factor of 1 represents general corrosion; i.e., $P_d = P_u$, and $d_{max} = 0$. The greater the (d_{max}), the greater the pitting factor.

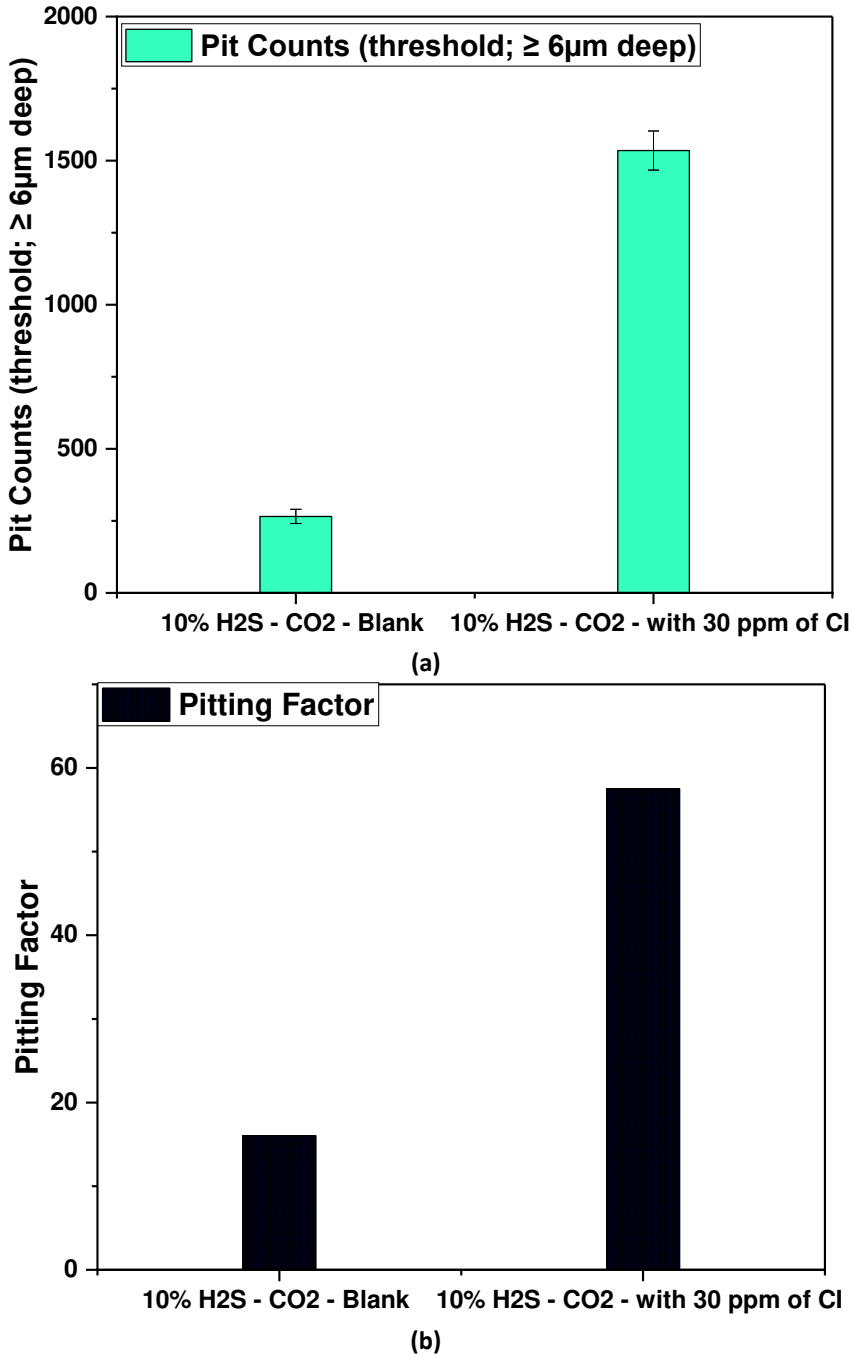

Figure 11: A graph of (a) pit density and (b) pitting factor showing the relative contribution of uniform and pitting corrosion to metal penetration of carbon steel in 10% H_2S - CO_2 after 48 h with 0 and 30 ppm of Cl.

4. Conclusions

This paper investigates the corrosion kinetics and behaviour of carbon steel in H_2S-containing corrosion environments with emphasis on FeS formation kinetics, interaction with corrosion inhibitor and corrosion damage mechanisms. Some of the key conclusions are highlighted below.

1. FeS (Mackinawite) formation kinetics have been shown to occur quickly without the requirement of significant availability of ferrous ions. This has been shown to occur within the first 0.5 – 1 h of interaction with dissolved H_2S gas due to the direct reduction of H_2S at the steel surface.

2. The fast kinetics of FeS formation led to an incompletely covered corrosion surface by FeS, with coverage almost replicating the distribution of ferrite – pearlite phases within the steel microstructure.

This has an impact of substantial reduction of uniform corrosion rate due to the blocking of active anodic sites by FeS formed.

3. FeS (macknawite) corrosion products quickly undergo a time-dependent morphological transformation with increasing exposure time, particularly in closed test systems. The main morphological form of FeS in the initial stages is amorphous.

4. The use of 30 ppm of CI (based on the reaction of an ethoxylated amine and a dicarboxylic ester) resulted in complex mechanisms of interaction of CI, FeS and the corrosion interface. The use of CI caused a delay in the FeS formation kinetics at the corrosion interface and restricts morphology to amorphous FeS. The fast kinetics of FeS formation prevented the availability of ferrous ions needed by the by the CI to form an effective corrosion barrier at the corrosion interface. This led to the establishment of a weak CI film which is easily displaced by the emerging FeS layer.

5. The competition between the CI layer and the FeS for interaction with the corroding interface acts to undermine the integrity of both CI film and FeS layer, leading to increased severity of pitting corrosion attack.

Data availability

The raw/processed data required to reproduce these findings cannot be shared at this time as the data also forms part of an ongoing study.

Credit authorship contribution statement

Frederick Pessu: Conceptualization, Methodology, Formal analysis, Investigation, Resources, Writing - original draft. **Richard Barker**: Writing - review & editing **Fakuen Chang**: Review & editing. **Tao Chen**: Writing - review & editing. . **Anne Neville**: Writing - review & editing and supervision

Declaration of Competing Interest

The authors declare that there is no conflict of interest.

Acknowledgement

The authors acknowledge the funding and support from Saudi Aramco and Chevron for this project.

5. References

1. D.W. Shoesmith, P. Taylor, M.G. Bailey, and D.G. Owen, "The Formation of Ferrous Monosulfide Polymorphs during the Corrosion of Iron by Aqueous Hydrogen Sulfide at 21°C", Journal of The Electrochemical Society, 127, 5 (1980): p. 1007-1015.

2. F. Pessu, R. Barker, and A. Neville, "Pitting and Uniform Corrosion of X65 Carbon Steel in Sour Corrosion Environments: The Influence of CO_2, H_2S, and Temperature", Corrosion, 73, 9 (2017): p. 1168-1183.

3. F. Pessu, Y. Hua, R. Barker, and A. Neville, "A Study of the Pitting and Uniform Corrosion Characteristics of X65 Carbon Steel in Different H_2S-CO_2-Containing Environments", Corrosion 74, 8 (2018): p. 886-902.

4. S.N. Smith. "Current understanding of corrosion mechanisms due to H_2S in oil and gas production environments", CORROSION, Paper no. 5485, (Dallas, TX: NACE International 2015, 2015).

5. M. Singer, B. Brown, A. Camacho, and S. Nešić, "Combined effect of carbon dioxide, hydrogen sulfide, and acetic acid on bottom-of-the-line corrosion", Corrosion, 67, 1 (2011): p. 015004-1-015004-16.

6. Y. Zheng, B. Brown, and S. Nešić, "Electrochemical study and modelling of H_2S corrosion of mild steel", Corrosion, 70, 4 (2013): p. 351-365.

7. J. Kittel, F. Ropital, F. Grosjean, E.M.M. Sutter, and B. Tribollet, "Corrosion mechanisms in aqueous solutions containing dissolved H_2S. Part 1: Characterisation of H_2S reduction on a 316L rotating disc electrode", Corrosion Science, 66, (2013): p. 324-329.

8. Y. Zheng, J. Ning, B. Brown, and S. Nešić, "Electrochemical Model of Mild Steel Corrosion in a Mixed H_2S/CO_2 Aqueous Environment in the Absence of Protective Corrosion Product Layers", Corrosion, 71, 3 (2015): p. 316-325.

9. H. Ma, X. Cheng, G. Li, S. Chen, Z. Quan, S. Zhao, and L. Niu, "The influence of hydrogen sulfide on corrosion of iron under different conditions", Corrosion Science, 42, 10 (2000): p. 1669-1683.

10. H.-H. Huang, W.-T. Tsai, and J.-T. Lee, "Corrosion morphology of A516 carbon steel in H_2S solution", Scripta Metallurgica et Materialia, 31, 7 (1994): p. 825-828.

11. P.H. Tewari and A.B. Campbell, "Dissolution of iron during the initial corrosion of carbon steel in aqueous H_2S solutions", Canadian Journal of Chemistry, 57, 2 (1979): p. 188-196.

12. C. Zhang, V. Zahedi Asl, Y. Lu, and J. Zhao, "Investigation of the corrosion inhibition performances of various inhibitors for carbon steel in CO_2 and CO_2/H_2S environments", Corrosion engineering, science, and technology, 55, 7 (2020): p. 531-538.

13. J.A. Dougherty, Outlaw, Benjie T., Oude Alink, Bernardus A. , *Corrosion inhibition by ethoxylated fatty amine salts of maleated unsaturated acids*, 1996, Petrolite Corporation (St. Louis, MO): United States.

14. *Chapter 6 - Corrosion inhibitors*, in *Petroleum Engineer's Guide to Oil Field Chemicals and Fluids (Second Edition)*, J. Fink, Editor. 2015, Gulf Professional Publishing: Boston. p. 215-254.

15. ASTM Standard G46-94, Standard guide for examination and evaluation of pitting corrosion. ASTM International: West Conshohocken, PA, 2003.

16. F. Pessu, R. Barker, and A. Neville, "Understanding Pitting Corrosion Behavior of X65 Carbon Steel in CO_2-Saturated Environments: The Temperature Effect", Corrosion, 72, 1 (2015): p. 78-94.

17. S. Guo, L. Xu, L. Zhang, W. Chang, and M. Lu, "Corrosion of alloy steels containing 2% chromium in CO_2 environments", Corrosion Science, 63, (2012): p. 246-258.

18. B.M. Kermani and A. Morshed, "Carbon dioxide corrosion in oil and gas production: A compendium", Corrosion, 59, 08 (2003): p. 659-683.

19. J.L. Crolet, N. Thevenot, and S. Nesic, "Role of Conductive Corrosion Products in the Protectiveness of Corrosion Layers", Corrosion, 54, 3 (1998): p. 194-203.

20. D.R. Morris, L.P. Sampaleanu, and D.N. Veysey, "The Corrosion of Steel by Aqueous Solutions of Hydrogen Sulfide", Journal of The Electrochemical Society, 127, 6 (1980): p. 1228-1235.

21. Y.-S. Choi, S. Nesic, and S. Ling, "Effect of H_2S on the CO_2 corrosion of carbon steel in acidic solutions", Electrochimica Acta, 56, 4 (2011): p. 1752-1760.

22. P.W. Bolmer, "Polarization of iron in H_2S-NaHS buffers", Corrosion, 21, 3 (1965): p. 69-75.

23. C.A.R. Silva, X. Liu, and F.J. Millero, "Solubility of Siderite ($FeCO_3$) in NaCl Solutions", Journal of Solution Chemistry, 31, 2 (2002): p. 97-108.

24. W. Davison, "The solubility of iron sulphides in synthetic and natural waters at ambient temperature", Aquatic Sciences, 53, 4 (1991): p. 309-329.

25. S.N. Esmaeely, B. Brown, and S. Nešić, "Verification of an Electrochemical Model for Aqueous Corrosion of Mild Steel for H_2S Partial Pressures up to 0.1 MPa", Corrosion 73, 2 (2017): p. 144-154.

26. A. Singh, Y. Lin, I.B. Obot, and E.E. Ebenso, "Macrocyclic inhibitor for corrosion of N80 steel in 3.5% NaCl solution saturated with CO_2", Journal of Molecular Liquids, 219, (2016): p. 865-874.

27. M. Schütze, R.W. Cahn, and E.J. Kramer, *Corrosion and Environmental Degradation: A Comprehensive Treatment*. 2000: Wiley-VCH.

28. H.-h. Zhang, X. Pang, and K. Gao, "Localized CO_2 corrosion of carbon steel with different microstructures in brine solutions with an imidazoline-based inhibitor", Applied Surface Science, 442, (2018): p. 446-460.

29. C.I. Pearce, R.A.D. Pattrick, and D.J. Vaughan, "Electrical and Magnetic Properties of Sulfides", Reviews in Mineralogy and Geochemistry, 61, 1 (2006): p. 127-180.

30. J. Han, B.N. Brown, and S. Nešić, "Investigation of the galvanic mechanism for localized carbon dioxide corrosion propagation using the artificial pit technique", Corrosion, 66, 9 (2010): p. 12.

31. A.S.T.M. International, *ASTM G46-94 Standard Guide for Examination and Evaluation of Pitting Corrosion*, 2005, ASTM International: West Conshohocken, PA. p. 7.